Functionalized nanoscale oil bodies for targeted delivery of a hydrophobic drug

2011 Nanotechnology 22 415102

(http://iopscience.iop.org/0957-4484/22/41/415102)

Nanotechnology **22** (2011) 415102 (9pp) doi:10.1088/0957-4484/22/41/415102

Functionalized nanoscale oil bodies for targeted delivery of a hydrophobic drug

Chung-Jen Chiang, Che-Chin Lin, Tzu-Li Lu and Hesin-Fu Wang

Department of Medical Laboratory Science and Biotechnology, China Medical University, 91 Hsue-Shih Road, Taichung 40402, Taiwan

E-mail: cjchiang@mail.cmu.edu.tw

Received 6 July 2011, in final form 10 August 2011
Published 14 September 2011
Online at stacks.iop.org/Nano/22/415102

Abstract

Effective formulations of hydrophobic drugs for cancer therapies are challenging. To address this issue, we have sought to nanoscale artificial oil bodies (NOBs) as an alternative. NOBs are lipid-based particles which consist of a central oil space surrounded by a monolayer of oleosin (Ole)-embedded phospholipids (PLs). Ole was first fused with the anti-HER2/*neu* affibody (Ole–ZH2), and the resulting hybrid protein was overproduced in *Escherichia coli*. ZH2-displayed NOBs were then assembled by sonicating the mixture containing plant oil, PLs, and isolated Ole–ZH2 in one step. To illustrate their usefulness, functionalized NOBs were employed to encapsulate a hydrophobic anticancer drug, Camptothecin (CPT). As a result, these CPT-loaded NOBs remained stable in serum and the release of CPT at the non-permissive condition exhibited a sustained and prolonged profile. Moreover, plain NOBs were biocompatible whereas CPT-loaded NOBs exerted a strong cytotoxic effect on HER2/*neu*-positive cells *in vitro*. Administration of xenograft nude mice with CPT-loaded NOBs also led to the regression of solid tumors in an effective way. Overall, the result indicates the potential of NOBs for targeted delivery of hydrophobic drugs.

(Some figures in this article are in colour only in the electronic version)

1. Introduction

Cancer appears to be the most life-threatening disease in humans. The breakthrough of cancer nanotechnology offers a great promise for combating this disease [1]. One promising strategy is to functionalize the carriers encapsulated with antitumor drugs. This is commonly approached by conjugation of the drug-loaded carriers with a ligand that binds to the tumor-cell-specific biomarker. After administration of these functional carriers, the chemotherapeutic entity is selectively delivered to tumorous sites. This results in an increase in drug efficacy and a decrease in the drug toxicity to normal cells [2]. Nanoparticles are particularly useful for targeted delivery of many drugs, which usually can improve pharmacokinetic properties and the therapeutic index of drugs [3]. Among many nanocarriers, polymeric nanoparticles and liposomes are two representative examples for various drug formulations [4, 5]. Although the results are encouraging, the complexity still exists in the optimization of many biophysicochemical parameters for drug formulations based on these two carriers, particularly for hydrophobic drugs [6, 7]. The problem frequently associated with the administration of hydrophobic drug-loaded nanocarriers is low bioavailability and high local concentration of drugs at the site of the aggregate deposition [8, 9]. As well recognized, many anticancer pharmaceuticals of high efficacy are poorly soluble. Therefore, the key issue at present is how to make targeted delivery of hydrophobic agents via oral or intravenous administration effective.

To address this issue, we have recently explored artificial oil bodies (AOBs) as a potential drug delivery carrier [10, 11]. Like its natural counterpart (e.g. plant seed oil body), AOBs are mainly composed of a triacylglycerol (TAG) matrix (see figure 1). This oil matrix is surrounded by a monolayer of phospholipids (PLs) into which the structural protein, such as oleosin (Ole), is embedded [12, 13]. The structure of Ole comprises a central lipophilic core that is anchored onto PLs and two terminal hydrophilic domains that protrude outwards [14]. Bearing a negative charge, the two protruding domains provide an electronegative repulsion force to maintain

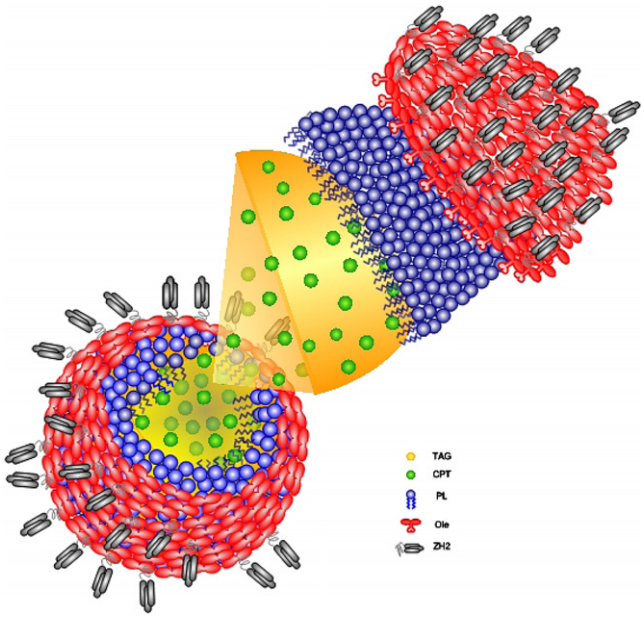

Figure 1. Schematic illustration of the structure of NOBs. NOBs could be functionalized by fusion of a bioactive motif (e.g. ZH2) with Ole. Upon self-assembly, the bioactive motif is displayed on the surface of NOBs. For clear illustration, only parts of Ole with linkage to ZH2 were shown.

the integrity of individual AOB [15, 16]. Technically, AOBs can be created by self-assembly of biomaterials consisting of plant oils, PLs, and Ole in one step [17]. Their size can be tailored to reach the nanoscale by varying the ratio of the matrix oil to Ole [11]. In particular, AOBs present to be a superior matrix for the surface display of the passenger motif that is fused with the N- or C-terminus of Ole. This remarkable feature ushers in many biotechnological applications based on AOBs [18–20].

AOBs essentially consist of natural lipids with a hydrophobic core. This renders it appealing for encapsulation of hydrophobic agents. Therefore, the preliminary study has been undertaken to explore the feasibility of AOBs for selective delivery of a cargo dye into tumor cells [10, 11]. The approach was based on the fusing of a small domain consisting of the arginine–glycine–aspartate (RGD) motif or a bivalent anti-HER2 affibody (denoted as ZH2) with Ole. After overproduction in *Escherichia coli*, the resulting protein (e.g. Ole fused to either RGD or ZH2) was recovered to assemble nanoscale AOBs (NOBs). Entrapped with a hydrophobic fluorescence dye, these functionalized NOBs were applied to tumor cells *in vitro*. As a result, RGD- or ZH2-displayed NOBs were able to target and penetrate tumor cells overexpressing $\alpha_v\beta_3$ integrin and HER2/*neu*, respectively. The internalization efficiency could reach as high as 80%–90%. Moreover, the internalized NOBs disintegrate at the non-permissive pH (e.g. in acidic endosomes) over time, resulting in the release of the cargo dye. The release profile showed a sustained and prolonged curve. All these findings clearly indicate the potential of NOBs as a drug delivery carrier.

In this study, we continued our efforts to explore the usefulness of NOBs for targeted delivery of hydrophobic drugs. A potent anticancer agent, Camptothecin (CPT), was chosen for demonstration. CPT is a cytotoxic alkaloid that is first isolated from *Camptotheca acuminate*. This drug functions to inhibit the activity of topoisomerase I during the S phase of the cell cycle [21]. Nevertheless, CPT is poorly absorbed after oral administration and shows highly variable pharmacokinetics [22, 23]. To illustrate, NOBs were functionalized by displaying ZH2 on their surface. ZH2-displayed NOBs were exploited for CPT formulations and detailed characterization was further carried out. For the first time, the result indicates that functionalized NOBs are promising for targeted delivery of the hydrophobic anticancer drug to tumor cells both *in vitro* and *in vivo*. This may open a new avenue in the field of cancer nanotechnology.

2. Experimental method

2.1. Bacteria culturing and protein production

Plasmid pJO1-Ole–ZH2 contains the *N*-terminal fusion of Ole with ZH2 under the control of the T7 promoter [11]. Similar to plasmid pJO1-Ole–ZH2, plasmid pJO1-Ole serves as a control and carries Ole alone. The two plasmids were transformed into *E. coli* strain BL21(DE3) to obtain strain BL21/pJO1-Ole–ZH2 and BL21/pJO1-Ole, respectively. Shake-flask cultures of bacterial strains were carried out in a similar way as reported previously [11]. In brief, bacteria were harvested by centrifugation after induction and then resuspended in 10 mM sodium phosphate buffer (PBS) at pH 7.5. Following disruption by sonication, bacterial proteins were collected by centrifugation and were analyzed by sulfate polyacrylamide gel electrophoresis (SDS-PAGE). The quantitative amount of recombinant proteins was determined using the Image Analyzer GA90000 (UVItec, UK).

2.2. Encapsulation of CPT by self-assembled NOBs

Essentially following the previous report [11], NOBs were assembled in 1 ml PBS which contained 100 μg olive oil, 150 μg PLs and 100 μg purified Ole or Ole–ZH2 fusion protein at pH 7.5 and 4 °C. To encapsulate the drug, NOBs were prepared in the same way except that an indicated amount of CPT was added to the assembly solution. The mixture was then subjected to sonication with the amplitude set at 20% for 10 s (VCX750, Sonics & Materials Co., USA). After repeating three times on ice, CPT-loaded NOBs were collected by centrifugation and washed with PBS.

2.3. Fourier transform infrared spectroscopic (FTIR) analysis

The mechanistic interaction of CPT with NOBs was analyzed using the Digilab FTS3500 spectrophotometer (Bio-Rad, USA). The FTIR spectra of CPT formulations on KBr pellets were obtained in the region from 4000 to 650 cm^{-1}.

2.4. Differential scanning calorimetry (DSC)

The DSC analysis was carried out with a CSC 6300 microcalorimeter (Calorimetry Science Co., USA). Indium

was used for the calibration of melting point and heat of fusion. Under nitrogen purge, the instrument was operated within the range of 20–300 °C with a heating rate of 10 °C min^{-1}. The aluminum sample pan (Calorimetry Science Co., USA) was used as a standard while an empty pan served as a reference.

2.5. Morphology study

The morphology of CPT-loaded NOBs was visualized with an atomic force microscope (AFM) of NS4/D3100CL/Multi Mode (Digital Instrument, Germany). The AFM was performed in the tapping mode to investigate the surface morphology of NOBs in three dimensions. A drop of the CPT-loaded NOB suspension was cast onto the mica surface at room temperature. A cantilever was used for scanning with a nominal force constant of 20 N m^{-1}. In addition, CPT-loaded NOBs were also analyzed by transmission electron microscopy (TEM) with the model of JEOL JEM-1400 (Japan). The protocol for performing TEM essentially followed our recent report [11].

2.6. Particle size and zeta potential analysis

The mean particle size of CPT-loaded NOBs was determined by the laser light scattering method as reported previously [11]. Meanwhile, the polydispersity index (PI) and zeta potential of CPT-loaded NOBs were determined by a Zetasizer (HSA 3000, Malvern Instrument Ltd, UK). The particles were dispersed in water to obtain a proper scattering intensity before measurement. The zeta potential values were assessed by determining the particle electrophoretic velocity.

2.7. Drug loading and release study in vitro

The loading yield and released amount of CPT in NOBs were measured using a dialysis bag (membrane: Spectra/Por 12 000–14 000 MWCO, Spectrum Laboratories, USA) as described previously [11]. CPT-loaded NOBs (1 ml) placed in a dialysis bag were immersed in 0.01 M PBS (20 ml). The dialysis was conducted at 37 °C under constant stirring. At time intervals, aliquots of PBS (100 μl) were withdrawn and replenished by the same volume of fresh PBS. The content of CPT in the withdrawn PBS was measured (see below) and normalized to the initial weight encapsulated in NOBs. All experiments were performed in triplicate. Drug loading content and encapsulation efficiency were calculated as follows:

$$\text{Drug loading content \%} = \frac{\text{Weight of CPT in NOBs}}{\text{Weight of NOBs with CPT}} \times 100\%$$

$$\text{Encapsulation efficiency \%} = \frac{\text{Weight of CPT in NOBs}}{\text{Weight of feeding CPT}} \times 100\%.$$

2.8. Measurement of CPT

Released CPT was measured by a high performance liquid chromatography (HPLC) system which comprises a Waters 2795 Separations Module and a Waters 2996 Photodiode Array Detector (Waters, USA). Samples were analyzed using Mightysil RP-18 GP (Kanto, Japan) and detected at 254 nm with the mobile phase pumped at 1 ml min^{-1}. The mobile phase consisted of acetonitrile and water with the volume ratio at 30:70.

2.9. Cell culture

Human cancer cell lines, including MDA-MB-231 (ovarian), SKOV3 (ovarian), MCF7 (breast) and MCF7/Her18 (HER2-transfected stable cell line), were grown according to the previous report [11]. In brief, tumor cells were cultured at 37 °C in a humidified atmosphere (5%) in the presence of CO_2. The culture medium was changed every two days until cell confluence reached 80%. Cell concentration was calculated using a hemocytometer. For analyses, cells were resuspended and seeded into a 24-well plate to reach 1×10^5 cells per well.

2.10. In vitro assessment of cytotoxicity

Cell cytotoxicity of NOBs with or without CPT was assessed according to our previous report [11]. Tumor cells were cultured in a 96-well plate and treated with various CPT formulations. After removal of the supernatant, the cells were washed with PBS and incubated in DMEM with 10% WST-8 solution for 2 h. Based on a cell-counting kit (Dojindo Molecular Technologies, Inc.), the absorbance of each well was measured at 450 nm using a microplate reader (SpectraMax M2, Molecular Device, USA). Cell viability was calculated as the ratio of absorbance of NOB-treated cells relative to that of untreated cells.

2.11. Hemolysis assay

CPT formulations were incubated in diluted blood (1 ml) at 37 °C for 30 min. Subsequently, plasma was separated by centrifugation of blood-containing suspensions at 2000 rpm for 3 h. The amount of hemoglobin released due to hemolysis was measured spectrophotometrically at 543 nm (V530, Jasco, Japan). The hemolytic activity was calculated with reference to blank and completely hemolyzed samples (e.g. distilled water). Light microscopy (Nikon type E600, Japan) was used to characterize any abnormalities in the blood cells after incubation.

2.12. Antitumor activity in vivo

Animal experiments were carried out in agreement with the principles outlined by the Committee of China Medical University (no. 99-18-N). BALB/cAnN.Cg nude mice (four weeks old, female, and 20 g body weight) were purchased from the National Laboratory Animal Center in Taiwan and maintained under specific pathogen-free conditions in the Animal Center at China Medical University. The mouse tumor model was developed by injecting an SKOV3 cell suspension (0.1 ml) at 1×10^7 cells/mouse into the right flank of a nude mice mouse. Tumor nodules were allowed to grow to a volume >150 mm^3 before the treatment was initiated. Tumor-bearing

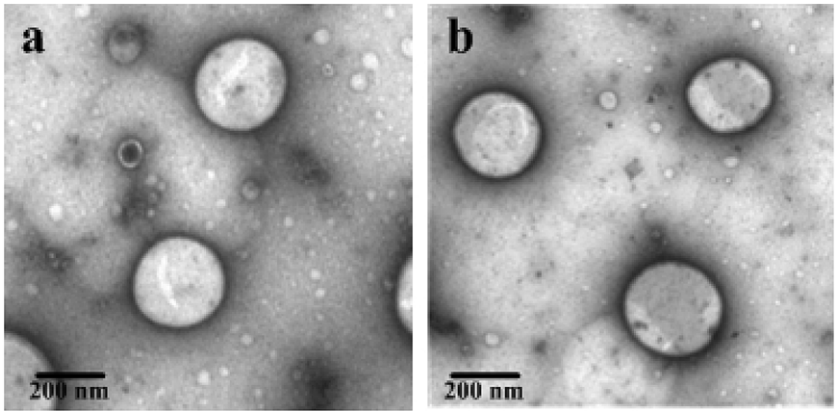

Figure 2. TEM images of (a) plain NOBs and (b) NOBs loaded with 500 μg ml^{-1} CPT.

Table 1. Characteristics of CPT-loaded NOBs. (Note: the size of nanoparticles was determined by the laser light scattering method. Symbols: NOB, plain NOB; F50, NOBs loaded with 50 μg ml^{-1} CPT; F100, NOBs loaded with 100 μg ml^{-1} CPT; and F500, NOBs loaded with 500 μg ml^{-1} CPT. ND = not detected.)

	CPT (μg ml^{-1})	Particle size (nm) $\pm$ SD	Polydispersity index (PI)	Zeta potential (mV) $\pm$ SD	Drug loading content (%)	Encapsulation efficiency (%)
NOB	0	247.9 ± 5.8	0.324 ± 0.021	-29.2 ± 2.3	ND	ND
F50	50	251.7 ± 8.7	0.154 ± 0.018	-24.1 ± 1.5	10.1 ± 2.5	69.7 ± 2.5
F100	100	253.7 ± 8.8	0.256 ± 0.065	-22.5 ± 1.2	19.3 ± 5.6	76.3 ± 4.5
F500	500	255.2 ± 19.2	0.219 ± 0.031	-14.1 ± 1.8	54.0 ± 9.2	85.9 ± 8.2

nude mice were randomly assigned to four groups and each group contained five mice. Tumor length and width were measured with a caliper and the tumor volume was calculated using the following equation:

$$\text{Tumor volume } (V) = \text{length} \times \text{width} \times \text{width}/2.$$

Prior to treatment, all mice were numbered and recorded for their initial weight and initial tumor volume. Animals were given two intratumorous injections of CPT formulations at an interval of three days per week. The administrated dose of CPT was 0.5 mg kg^{-1} of mouse body weight. The body weight and tumor volume for each mouse were then measured twice a week.

3. Results and discussion

3.1. Characterization of CPT-loaded NOBs

After encapsulation with CPT, NOBs were characterized with respect to their morphology, particle size, size distribution, surface charge and physical state. As visualized by TEM, NOBs with or without CPT assumed a spherical shape with the size reaching approximately 200 nm (figures 2(a) and (b)). Meanwhile, AFM shows that the shape of NOBs remained unaffected before and after encapsulation of CPT (figures 3(a) and (b)). Their size was in the range of 250–300 nm, in agreement with that measured by the laser light scattering (table 1). Note that TEM measures the diameter of subjects at the dehydrated state while AFM and laser light scattering determine the hydrodynamic diameter of subjects. Therefore, it leads to the discrepancy in the size of NOBs as measured with different methods. Overall, encapsulation of CPT has no effect on the size of NOBs.

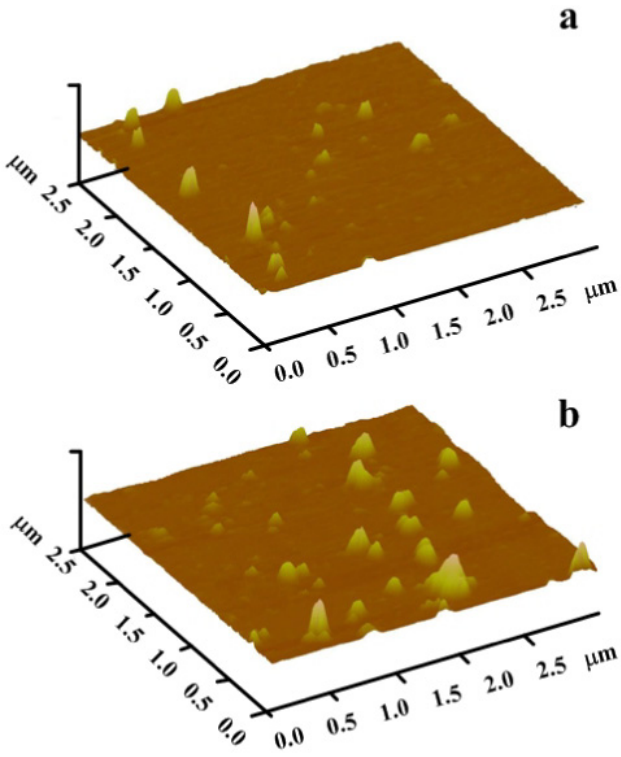

Figure 3. AFM micrographs of (a) plain NOBs and (b) NOBs loaded with 500 μg ml^{-1} CPT.

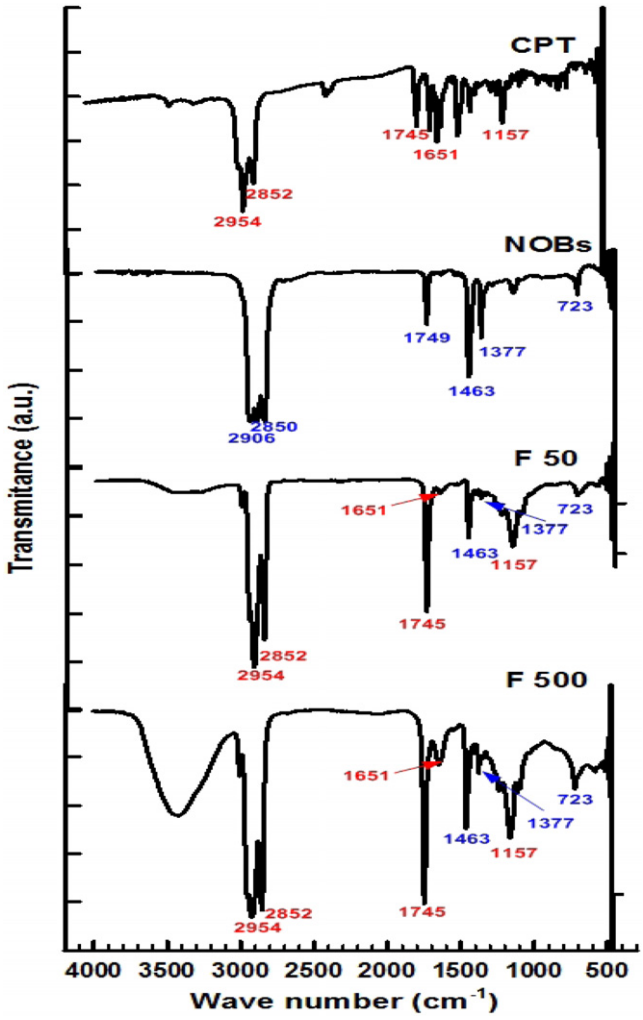

Figure 4. FTIR spectrum of CPT formulations. Symbols: CPT, plain CPT; NOBs, blank NOBs; F50, NOBs loaded with 50 μg ml^{-1} CPT; and F500, NOBs loaded with 500 μg ml^{-1} CPT.

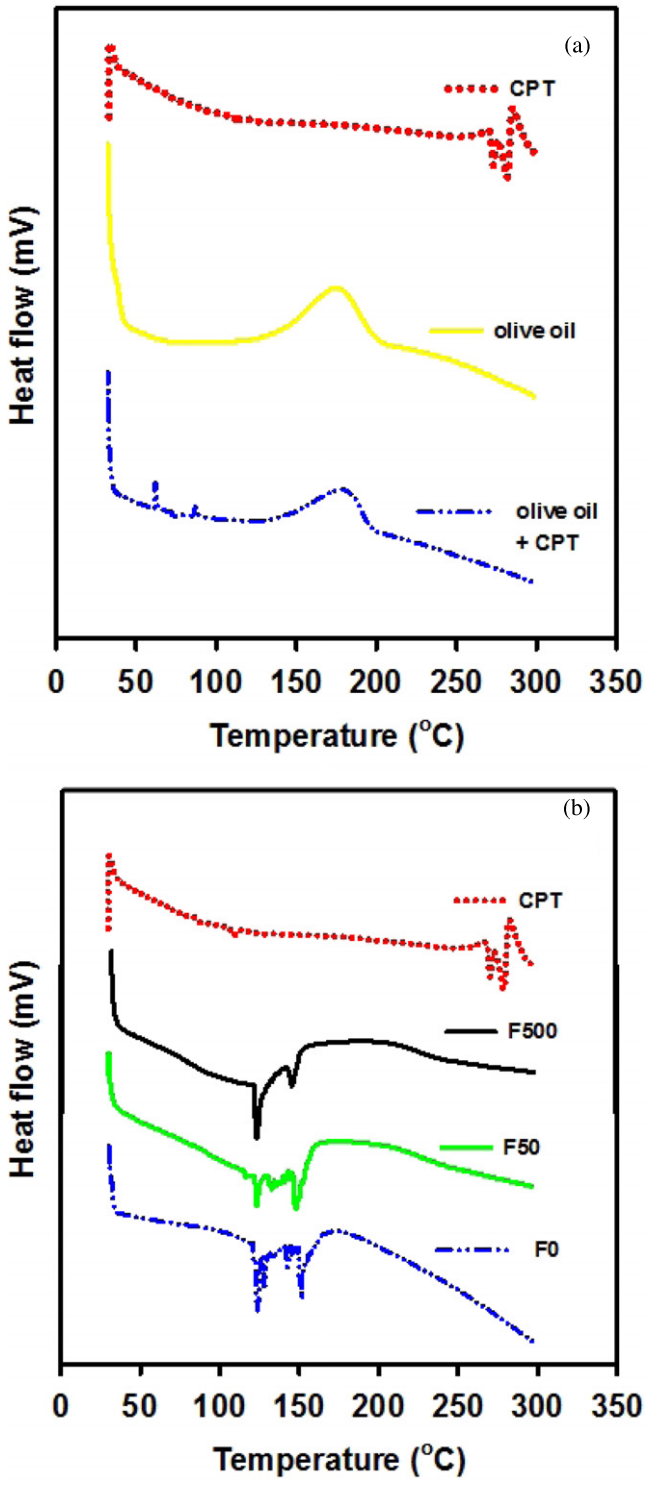

Figure 5. DSC thermograms of CPT formulation. (a) Plain CPT, plain olive oil and their mixture were processed for DSC analyses. (b) Various formulations of CPT in NOBs were analyzed. Refer to figure 4 for the symbols used.

The possible complexation of CPT with NOBs was further analyzed by FTIR. As depicted in figure 4, the FTIR spectra of plain CPT gave main characteristic peaks at 2954 and 2852 cm^{-1} (C–H stretching vibrations), 1745 and 1651 cm^{-1} (stretching vibration of ester and lactone carbonyl group) and 1157 cm^{-1} (C–N stretching vibration of benzene ring). The typical FTIR spectra of plain NOBs showed the prominent peaks arising from C–H (2954, 2906 and 2852 cm^{-1}) and C=O (1749 cm^{-1}) stretch vibrations, C–H deformation (1463 cm^{-1}) and $(CH_2)_n$, ($n > 4$) (723 cm^{-1}) bonding [24]. Upon encapsulation of CPT into NOBs, the characteristic peaks appearing in the spectra were the combination of those for plain CPT and plain NOBs and no extra peaks occurred. This result is consistent with the observation as reported previously [25]. It indicates an insignificant interaction between CPT and NOBs.

To investigate the physical state of CPT in NOBs, the DSC assay was carried out. Figure 5(a) shows that the DSC thermogram of plain CPT gave a characteristic melting peak at 270 °C. This endothermic peak disappeared when CPT was mixed with olive oil or once encapsulated into NOBs (figure 5(b)). This result suggests that CPT is completely dissolved in NOBs and remains at the amorphous state according to the previous report [26].

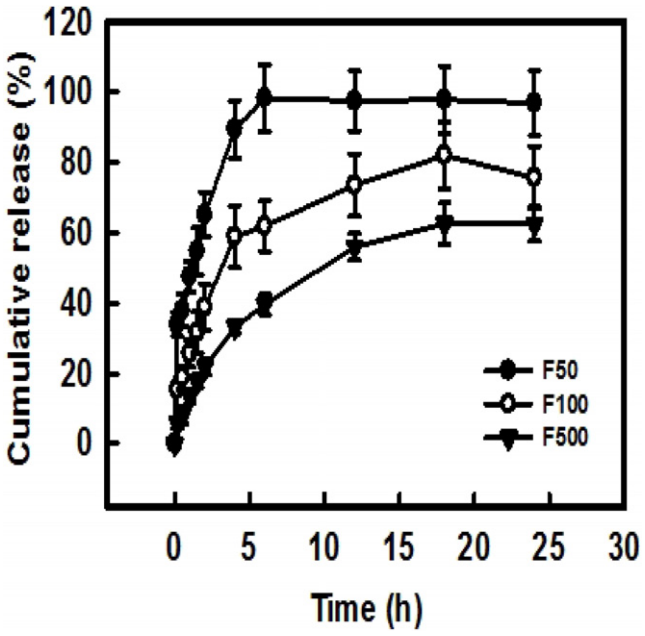

Figure 6. Drug release profile of CPT-loaded NOBs. CPT was loaded into NOBs with the concentration of 50 (F50), 100 (F100) and 500 μg ml^{-1} (F500). Consequently, CPT-loaded NOBs were analyzed for the drug release. The experiment was conducted in triplicate.

3.2. Loading capacity and release of CPT

A carrier with a high loading capacity is helpful to reduce the quantity of carriers for administration. Therefore, the CPT loading capacity of NOBs was investigated by the dialysis method as described. After encapsulation of various CPT into NOBs, the encapsulation efficiency was found to reach 70–85% (table 1).

Figure 6 shows the cumulative release profile of CPT from NOBs. The initial burst release was prominent in the first 5 h and reached more than 90%, 60% and 30% of the original CPT for F50, F100 and F500 formulations, respectively. After this burst release, it gave a constant and slow release profile of CPT. The released amount of CPT could account for 98% (F50), 80% (F100) and 60% (F500) of the original dose at the end of experiments. Overall, CPT-loaded NOBs exhibit a sustained and prolonged drug release profile as commonly reported [27, 28].

3.3. In vitro cytotoxicity study and hemolysis test

To target tumor cells overexpressing HER2/*neu*, NOBs were functionalized by the surface display of ZH2. HER2/*neu* belongs to the human epidermal growth factor receptor family [29] and its abnormal overexpression can lead to the progression of aggression of tumors [30]. The further investigation was conducted to study the cytotoxic effect of CPT-loaded NOBs on tumor cells. CPT was very toxic to cells as expected (figure 7(a)). Consistent with our recent report [11], ZH2-displayed NOBs free of CPT exhibited no toxicity toward cells (figure 7(b)). The result indicates the biocompatibility nature of NOBs. However, the viability of MCF17/Her18 cell (HER2/*neu*-positive) was drastically reduced after the cell was exposed to ZH2-displayed NOBs with CPT. In contrast, the MCF7 cell (HER2/*neu*-negative) was insensitive to CPT-loaded NOBs. This suggests that CPT toxicity could be shielded after encapsulation into NOBs. According to our recent report [11], ZH2-displayed NOBs could be selectively internalized into HER2/*neu*-positive cells with internalization efficiency reaching 90%. Therefore, the cytotoxic effect on HER2/*neu*-positive cells is mainly ascribed to the targeted delivery of CPT by NOBs via a ZH2-mediated internalization pathway. Moreover, the CPT-mediated cytotoxicity towards HER2/*neu*-positive cells was not cell-dependent. The viability of both MCF17/Her18 and SKOV3 cells (HER2/*neu*-positive) dropped markedly in response to the administrated dose of CPT (figure 7(b)). The dose of formulated CPT that reduced cell viability by 50% was estimated to be 45 μg ml^{-1}. The result clearly indicates the high efficiency of functionalized NOBs for targeted delivery of the anticancer drug.

Safety is a key issue in the evaluation of the quality and the potential clinical application of a drug delivery system. Therefore, the hemolysis study was conducted to investigate the potential *in vitro* irritation of CPT-loaded NOBs. The result showed that NOBs with or without CPT were well tolerable to erythrocytes and the amount of hemolysis was negligible (figure 7(c)). Moreover, there was no hemolytic or blood cell agglutination after incubation of erythrocytes with NOBs for 3 h *in vitro* (figure 7(d)). Taken together, it indicates the stability and safety of NOBs.

3.4. In vivo antitumor activity

The antitumor efficacy of CPT-loaded NOBs was evaluated in a xenograft tumor model. CPT was encapsulated into plain NOBs (NOB–CPT) and ZH2-displayed NOBs (ZH–NOB–CPT). All drug formulations were administered twice (on day 1 and day 5) per week. As shown in figure 8(a), a significant antitumor effect in mice was observed after treatment with ZH–NOB–CPT for 15 days. The infected tumors receiving the treatment of ZH–NOB–CPT started to regress on day 5, while a striking regression of tumors occurred on day 20. Consequently, the average tumor volume dropped to 45% of the initial tumor volume (figure 8(b)). In contrast, the average tumor volume in NOB–CPT-treated mice grew uncontrollably with time and finally doubled (figures 8(a) and (b)). The result suggests that ZH2-tagged NOBs are able to selectively deliver CPT into the HER2/*neu*-positive tumor site. Without ZH2, NOBs became not invasive and carried CPT could not be delivered into cancerous sites. In addition, administration of CPT in PBS buffer gave a marginal antitumor effect and the tumor size remained unchanged throughout the experiment (figure 8(b)). This is probably due to the toxicity of CPT.

The change in the body weight of tumor-bearing mice after injections was further examined. As revealed in figure 8(c), no significant difference in the body weight was observed for mice treated with ZH–NOB–CPT, NOB–CPT or PBS (control). The body weight loss was within the tolerable range (e.g. <5% of initial body weight). However, mice that received free CPT lost

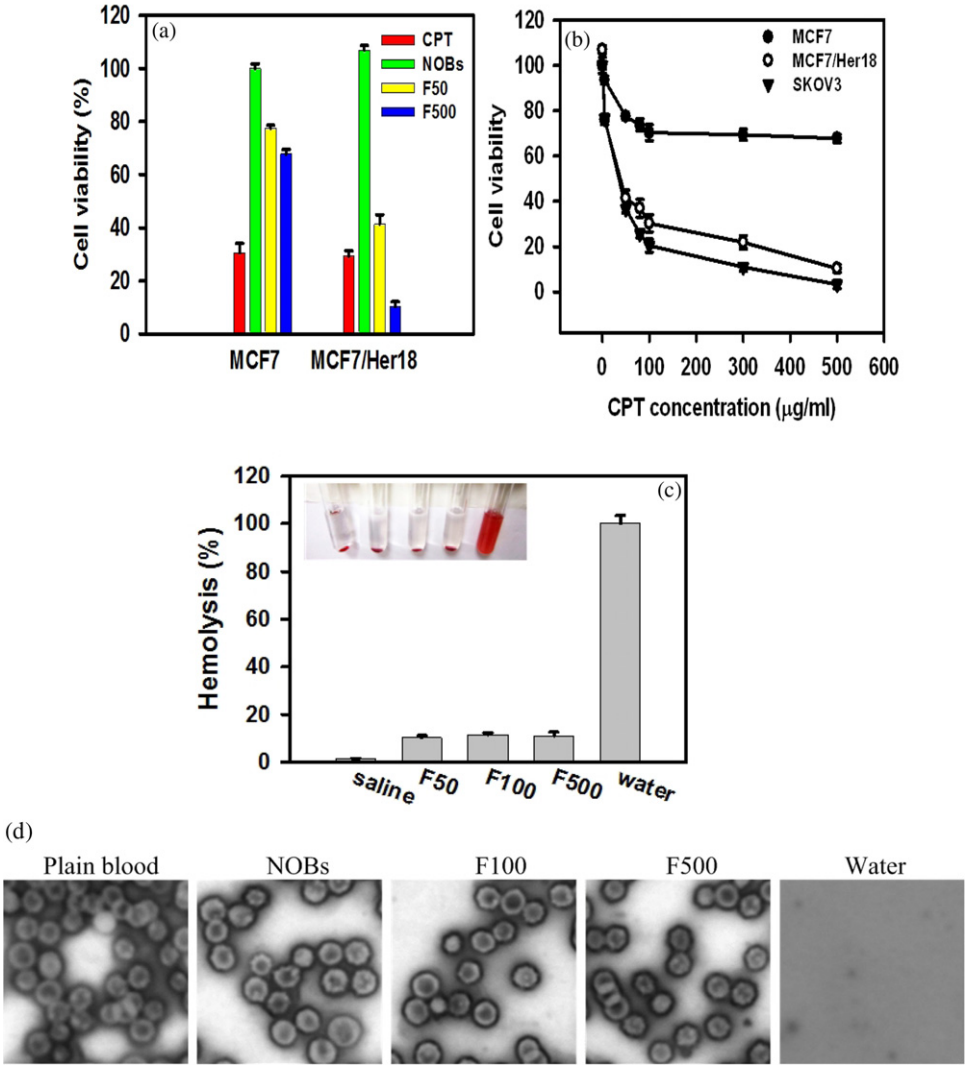

Figure 7. *In vitro* antitumor activity and stability of CPT-loaded NOBs. (a) Tumor cells were co-incubated with CPT formulations and assessed for their viability. Plain CPT (500 μg ml^{-1}) in olive oil was used as a control. The experiment was conducted in triplicate. (b) Viability of various tumor cells upon exposure to different doses of formulated CPT. The experiment was carried out with CPT-loaded NOBs in triplicate. (c) Hemolysis in erythrocytes after incubation with various CPT formulations. Saline was used as a negative control whereas distilled water was employed as a positive control. The experiment was conducted in triplicate. (d) Photographs of erythrocyte after incubation with various CPT formulations. Refer to figure 4 for the symbols used.

16% of their original body weight after administration for 20 days. This indicates the toxicity of free CPT. Upon entrapment of CPT into NOBs, the toxic effect of CPT could be sheltered.

4. Conclusion

Many potent antitumor drugs are poorly soluble. This makes the formulation of these hydrophobic drugs problematic and challenging. CPT is one of the well-known examples. Owing to its hydrolytic instability and adverse drug interaction, many efforts have been centered on the development of intralipid formulations of CPT [31]. Liposomes and polymeric micelles are proven useful for CPT delivery [32, 33]. Similarly, NOBs are lipid-based nanoparticles but comprise a central oil space that is surrounded by an Ole-embedded lipid monolayer (figure 1). No chemical modifications are required for reconstitution of functional NOBs. They are self-assembled and well reproducible upon mixing of Ole protein, plant oil and PLs in one step. In particular, NOBs could be functionalized simply by fusion of any bioactive motifs of interest with Ole (e.g. ZH2 in figure 1). Ole also confers on NOBs a negative surface charge [15], thereby contributing to the negative zeta potential (table 1). This feature is helpful to prevent undesired interaction of NOBs with non-target cells [34]. As illustrated, the central oil space of NOBs greatly facilitates the entrapment of hydrophobic CPT. These CPT-loaded NOBs are stable and exhibit a strong cytotoxic effect on HER2/*neu*-positive tumor cells both *in vitro* and *in vivo*. Moreover, the control-and-release nature of NOBs is acknowledged by their internalization through endosomes in which they disintegrate at acidic pH [11, 35]. In summary, we conclude that NOBs consisting of natural biomaterials are promising for targeted delivery of hydrophobic drugs.

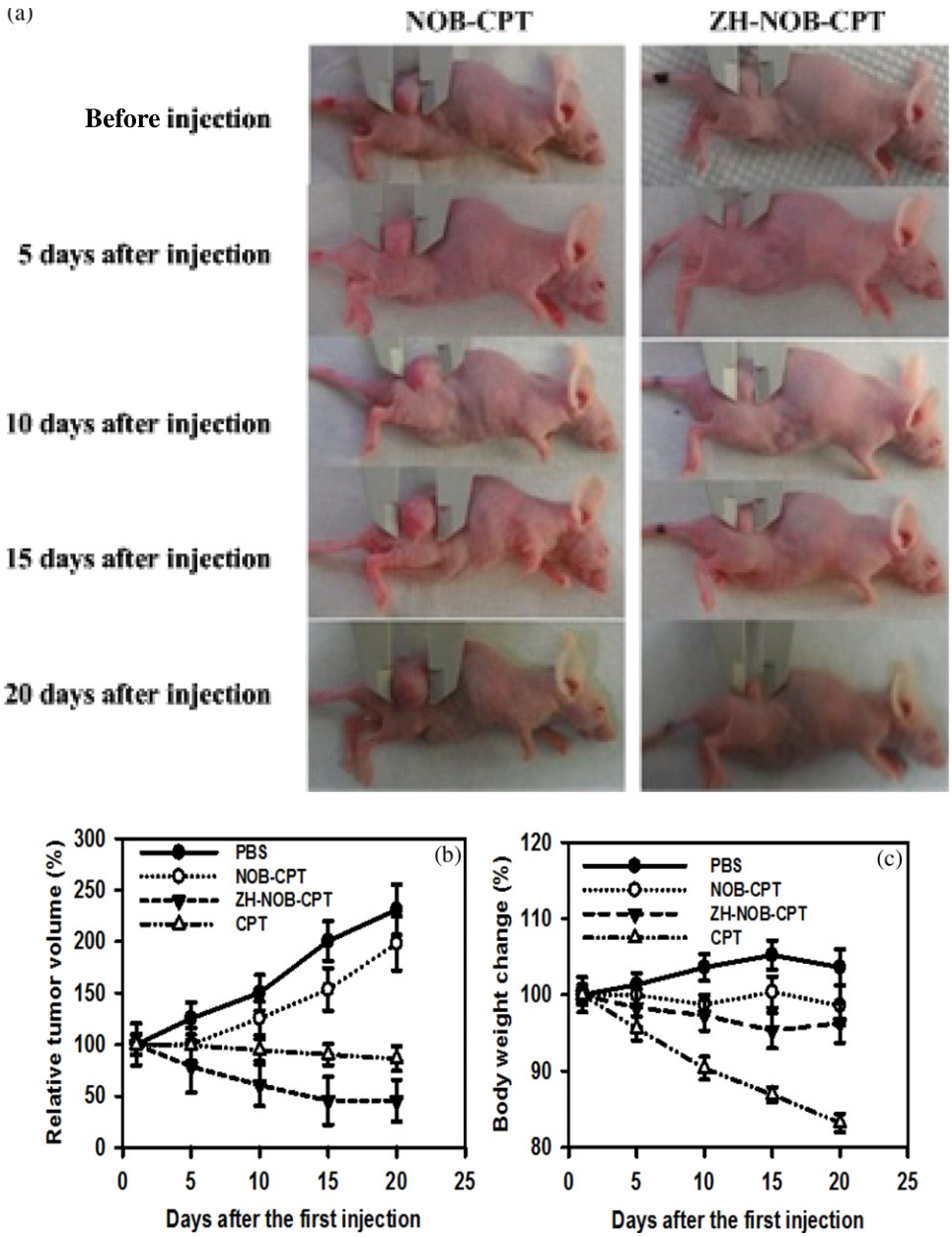

Figure 8. *In vivo* antitumor activity of CTP-loaded NOBs. Xenograft rude mice bearing SKOV3 tumor ($n = 5$) were injected with CPT-loaded NOBs as described. (a) Photographs of the change in tumor size after administration of ZH–NOB–CPT and NOB–CPT formulations. (b) Regression rate of tumor volume after administration of CPT formulations. PBS was used as a negative control. (c) Body weight change of mice after administration of CPT formulations.

Acknowledgments

We like to acknowledge the Instrument Center of R&D Office at China Medical University for technical assistance and Mr Jeffrey Conrad for a critical review of this manuscript. This work was supported by the National Science Council of Taiwan (NSC 99-2313-B-039-003-MY3) and China Medical University (98-C-11 and 98-N2-22).

References

[1] Farokhzad O C and Langer R 2009 Impact of nanotechnology on drug delivery *ACS Nano* **3** 16–20

[2] Cho K, Wang X, Nie S, Chen Z and Shin D M 2008 Therapeutic nanoparticles for drug delivery in cancer *Clin. Cancer Res.* **14** 1310–6

[3] Ferrari M 2005 Nanotechnology: opportunities and challenges *Nature Rev. Cancer* **5** 161–71

[4] Elbayoumi T A, Pabba S, Roby A and Torchilin V P 2007 Antinucleosome antibody-modified liposomes and lipid–core micelles for tumor-targeted delivery of therapeutic and diagnostic agents *J. Liposome Res.* **17** 1–14

[5] Zhang L, Chan J M, Gu F X, Rhee J W, Wang A Z, Radovic-Moreno A F, Alexis F, Langer R and Farokhzad O C 2008 Self-assembled lipid-polymer hybrid nanoparticles: a robust drug delivery platform *ACS Nano* **8** 1696–702

[6] Andresen T L, Jensenb S S and Jørgensen K 2005 Advanced strategies in liposomal cancer therapy: problems and prospects of active and tumor specific drug release *Prog. Lipid Res.* **44** 68–97
[7] Torchilin V P 2007 Micellar nanocarriers: pharmaceutical perspectives *Pharm. Res.* **24** 1–16
[8] Fernandez A M *et al* 2001 *N*-Succinyl-(*β*-alanyl-l-leucyl-l-alanyl-l-leucyl)doxorubicin: an extracellularly tumor-activated prodrug devoid of intravenous acute toxicity *J. Med. Chem.* **44** 3750–3
[9] Lipinski C A, Lombardo F, Dominy B W and Feeney P J 2000 Experimental and computational approaches to estimate solubility and permeability in drug discovery and development settings *Adv. Drug Deliv. Rev.* **46** 3–36
[10] Chiang C J, Chen C J, Chang C H and Chao Y P 2010 Selective delivery of cargo entities to tumor cells by nanoscale artificial oil bodies *J. Agric. Food Chem.* **58** 11695–702
[11] Chiang C J, Lin L J, Lin C C, Chang C H and Chao Y P 2011 Selective internalization of self-assembled artificial oil bodies by HER2/neu-positive cells *Nanotechnology* **22** 015102
[12] Huang A H 1996 Oleosins and oil bodies in seeds and other organs *Plant Physiol.* **110** 1055–61
[13] Napier J A, Stobart A K and Shewry P R 1996 The structure and biogenesis of plant oil bodies: the role of the ER membrane and the oleosin class of proteins *Plant Mol. Biol.* **31** 945–56
[14] Tzen J T C, Lie G C and Huang A H 1992 Characterization of the charged components and their topology on the surface of plant seed oil bodies *J. Biol. Chem.* **267** 15626–34
[15] Tzen J T C and Huang A H 1992 Surface structure and properties of plant seed oil bodies *J. Cell Biol.* **117** 327–35
[16] Tzen J T C, Chuang R L, Chen J C and Wu L S 1998 Coexistence of both oleosin isoforms on the surface of seed oil bodies and their individual stabilization to the organelles *J. Biochem.* **123** 318–23
[17] Peng C C, Lin I P, Lin C K and Tzen J T C 2003 Size and stability of reconstituted sesame oil bodies *Biotechnol. Prog.* **19** 1623–6
[18] Chiang C J, Chen H C, Chao Y P and Tzen J T C 2005 Efficient system of artificial oil bodies for functional expression and purification of recombinant nattokinase in *Escherichia coli* *J. Agric. Food Chem.* **53** 4799–804
[19] Chiang C J, Chen H C, Kuo H F, Chao Y P and Tzen J T C 2006 A simple and effective method to prepare immobilized enzymes using artificial oil bodies *Enzyme Microbial Technol.* **39** 1152–8
[20] Chiang C J, Chen H C, Chao Y P and Tzen J T C 2007 One-step purification of insoluble hydantoinase overproduced in *Escherichia coli Protein Express Purif.* **52** 14–8
[21] Shao R G, Cao C X, Shimizu T, O'Connor P M, Kohn K W and Pommier Y 1997 Abrogation of an S-phase checkpoint and potentiation of Camptothecin cytotoxicity by 7-hydroxystaurosporine (UCN-01) in human cancer cell lines, possibly influenced by p53 function *Cancer Res.* **57** 4029–35
[22] Garcia-Carbonero R and Supko J G 2002 Current perspectives on the clinical experience, pharmacology, and continued development of the Camptothecins *Clin. Cancer Res.* **8** 641–61
[23] Soepenberg O, Sparreboom A and Verweij J 2003 The alkaloids: clinical studies of Camptothecin and derivatives *Alkaloids Chem. Biol.* **60** 1–50
[24] Lacey D J, Wellner N, Beaudoin F, Napier J A and Shewry P R 1998 Secondary structure of oleosins in oil bodies isolated from seeds of safflower (*Carthamus tinctorius* L.) and sunflower (*Helianthus annuus* L.) *Biochem. J.* **334** 469–77
[25] Wenkai T, Wang L and D'Souza M J 2003 Evaluation of PLGA microspheres as delivery system for antitumor agent-Camptothecin *Drug Dev. Ind. Pharm.* **29** 745–756
[26] Barreiro-Iglesias R, Bromberg L, Temchenko M, Hatton T A, Concheiro A and Alvarez-Lorenzo C 2004 Solubilization and stabilization of Camptothecin in micellar solutions of pluronic-*g*-poly(acrylic acid) copolymers *J. Control. Release* **97** 537–49
[27] Kim G Y, Tyler B M, Tupper M M, Karp J M, Langer R S, Brem H and Cima M J 2007 Resorbable polymer microchips releasing BCNU inhibit tumor growth in the rat 9L flank model *J. Control. Release* **123** 172–8
[28] Yang Z, Zhang Y, Markland P and Yang V C 2002 Poly(glutamic acid) poly(ethylene glycol) hydrogels prepared by photoinduced polymerization: synthesis, characterization, and preliminary release studies of protein drugs *J. Biomed. Mater. Res.* **62** 14–21
[29] Hung M C and Lau Y K 1999 Basic science of HER2/*neu*: a review *Semin. Oncol.* **26** 51–59
[30] Citri A and Yarden Y 2006 EGF-ERBB signalling: towards the systems level *Nature Rev. Mol. Cell Biol.* **7** 505–16
[31] Venditto V J and Simaneck E E 2010 Cancer therapies utilizing the Campothcins: a review of the *in vivo* literature *Mol. Pharmacol.* **7** 307–49
[32] Sugarman S M, Zou Y Y, Wasan K, Poirot K, Kumi R, Reddy S and Perez-Soler R 1996 Lipid-complexed Camptothecin: formulation and initial biodistribution and antitumor activity studies *Cancer Chemother. Pharmacol.* **37** 531–8
[33] Kawano K, Watanabe M, Yamamoto T, Yokoyama M, Opanasopit P, Okano T and Maitani Y 2006 Enhanced antitumor effect of Camptothecin loaded in long-circulating polymeric micelles *J. Control. Release* **112** 329–32
[34] Suh W, Han S O, Yu L and Kim S W 2002 An angiogenic, endothelial-cell-targeted polymeric gene carrier *Mol. Ther.* **6** 664–72
[35] Ohkuma S and Poole B 1978 Fluorescence probe measurement of the intralysosomal pH in living cells and the perturbation of pH by various agents *Proc. Natl Acad. Sci. USA* **75** 3327–31